Contributions to Mineralogy and Petrology (2025) 180:32
https://doi.org/10.1007/s00410-025-02216-6

ORIGINAL PAPER

Mush system heterogeneities control magma composition and eruptive style on the Ocean Island of El Hierro, Canary Islands

Claudia Prieto-Torrell[1,2] · Helena Albert[1,2] · Meritxell Aulinas[1,2] · Eloi González-Esvertit[1,2,3] · Ilenia Arienzo[4] · Guillem Gisbert[1,2] · Valentin R. Troll[5] · Jose-Luis Fernandez-Turiel[3] · Alejandro Rodriguez-Gonzalez[6] · Francisco-Jose Perez-Torrado[6]

Received: 30 October 2024 / Accepted: 18 March 2025

Abstract
The study of recent eruptions in Ocean Islands (OIs) provides a unique window into the magma dynamics governing their plumbing systems and the mechanisms leading to eruptions. Here we present an integrated approach to unravel the dynamics of magmatic plumbing systems through detailed spatial, petrological, and geochemical characterisation of volcanic products ranging from crystal-rich ankaramitic lavas to trachytic tephras. We focus on the textural and geochemical spatial variations of 42 Holocene subaerial eruptions at the OI of El Hierro (Canary Islands), as well as on their petrogenetic significance for magmatic evolution and plumbing system architecture. Integrating geochemical data within fractional crystallisation modelling and mass balance calculations reveals that ankaramitic and porphyritic lavas with phenocryst modal abundances > 10 vol% result from melt extraction and crystal accumulation. Aphyric to sub-aphyric eruption products and porphyritic lavas with phenocryst modal abundances < 10 vol% usually follow fractional crystallisation trajectories that start at ~10 wt% MgO. Periodic extraction of evolved melt from crystal mushes likely led to the occurrence of minor trachytic eruptions, which are difficult to reconcile with simple closed system fractional crystallisation trends. A complex, heterogeneous crustal mush system beneath El Hierro is, in fact, the most reliable scenario to explain the wide range of textures, whole-rock and mineral compositions, and the overall surface distribution of vents and eruptive styles displayed by the Holocene volcanism on the island. Our integrated findings highlight the importance of a combined field, petrological, and geochemical study to decipher plumbing system dynamics of OI magmatism. The results allow us to put forward an updated conceptual model of the current plumbing architecture of El Hierro's volcanic system during the Holocene.

Keywords Ocean Island Basalts · Monogenetic eruptions · Melt extraction · Crystal accumulation · Crystal mush

Communicated by Gordon Moore.

✉ Claudia Prieto-Torrell
c.prieto-torrell@ub.edu

1 Department of Mineralogy, Petrology and Applied Geology, University of Barcelona, 08028 Barcelona, Spain

2 Geomodels Research Institute, University of Barcelona, 08028 Barcelona, Spain

3 Geosciences Barcelona (GEO3BCN-CSIC), 08028 Barcelona, Spain

4 Istituto Nazionale di Geofisica e Vulcanologia, Sezione di Napoli Osservatorio Vesuviano, 80124 Naples, Italy

5 Department of Earth Sciences, Natural Resources & Sustainable Development (NRHU), Uppsala University, 75236 Uppsala, Sweden

6 Instituto de Estudios Ambientales y Recursos Naturales (i-UNAT), University of Las Palmas de Gran Canaria, Las Palmas de Gran Canaria 35017, Spain

Published online: 23 April 2025

Introduction

Ocean Islands (OIs) are key settings for understanding lithospheric processes that control magma generation, transport, and eruption triggers in volcanic islands (e.g., O'Hara 1998; Humphreys and Niu 2009; White 2010; Niu et al. 2011). They lack the tectono-metamorphic complexity of most plate boundary zones and, accordingly, investigations on OIs have historically provided more direct insights into both ancient and active oceanic intraplate geodynamics (McKenzie and O'Nions 1983). Generally, OIs are characterised by transcrustal magmatic plumbing systems with complex architectures, comprising vertically interconnected storage zones where repeated melt injections and interactions between mantle-derived and crustal magmas occur (e.g., Sparks et al. 2019). OIs represent important areas of heat and mass transfer within the Earth's crust and constitute regional heterogeneities in the mechanical properties and overall strength of the lithosphere (Davies 1999). A comprehensive understanding of such complex systems profit from multidisciplinary investigations (e.g., petrological and geochemical studies, numerical modelling, and geophysical surveys), to provide insights into processes operating from mantle or lower-crustal magma generation and segregation zones to the common magma ponding in upper crustal reservoirs (e.g., Bons et al. 2004; Peltier et al. 2009; Dayton et al. 2023).

Over the past years, a growing number of inconsistencies in conceptual models of magma reservoirs in different settings have fostered an increasingly refined view, involving an advancement from simple *big tank* models to sophisticated *crystal mush* models (Cashman et al. 2017; Cooper 2017; Boulanger and France 2023). The latter assume that magma reservoirs mostly consist of a crystal-liquid mixture where crystals represent more than ~40–50% of the volume, and have been acknowledged to be more consistent with petrological (e.g., Albert et al. 2022), numerical modelling (e.g., Bergantz et al. 2015), and geophysical evidence (e.g., Lees 2007). Mush systems in various settings are controlled by processes such as filter pressing or compaction-driven melt segregation that ultimately trigger melt extraction and physicochemical changes in the leftover mush (Anderson et al. 1984; McKenzie 1984; Marsh 1996; Sisson and Bacon 1999; Caracciolo et al. 2020; Petrone et al. 2022). However, the interplay between fractional crystallisation, melt extraction, and crystal accumulation processes under the *crystal mush* framework in OI settings still has to be fully explored, which we address through investigating the Holocene eruption record on El Hierro island.

The Canary Islands have historically been considered an exceptional natural laboratory for understanding the processes that operate from source to surface and are responsible for magma generation, transport, and storage (e.g., Hoernle and Schmincke 1993; Hansteen et al. 1998; Carracedo et al. 2001; Manconi et al. 2009; Aulinas et al. 2010; Deegan et al. 2012; Dayton et al. 2023). Here we focus on the magmatic plumbing system of El Hierro, the westernmost and youngest island of the Canaries, because it displays a complex plumbing system where fractional crystallisation, magma mixing, and crystal recycling processes coexist (Manconi et al. 2009; Stroncik et al. 2009; Longpré et al. 2014; Klügel et al. 2015; Taracsák et al. 2019; Ubide et al. 2022). El Hierro exhibits crystal-rich ankaramitic lavas with crystal contents up to 51 vol% (Prieto-Torrell et al. 2024), as well as a wide spectrum of textures and geochemical compositions of erupted magmas ranging from picrites to trachytes (Carracedo et al. 2001). Through the investigation of 42 Holocene subaerial eruptions, we provide a detailed spatial, petrological, and geochemical characterisation of volcanic products, integrated with mass balance calculations and fractional crystallisation thermodynamic modelling, to assess the different degrees of crystal accumulation and melt extraction experienced by magmas within the El Hierro plumbing system. Investigating the magmatic plumbing system behaviour of the Holocene volcanism allows characterisation of governing magmatic processes and to link these to eruptive dynamics over a meaningful period of time, i.e. sufficient to recognise temporal relationships that continue to the present day. This in turn will aid in creating sensible current and future predictive scenarios to help hazard responses in the region. Integrating our results on texture, composition, and eruptive style with the recently updated geological map of the Holocene volcanism at El Hierro (Rodriguez-Gonzalez et al. 2024), we now provide new insights into the magma plumbing architecture beneath the island.

Geological setting

El Hierro is the youngest active volcanic system in the Canarian Archipelago. The subaerial part of the island was formed by the superimposition of monogenetic volcanoes that constructed three main volcanic units: Tiñor volcano (1.12–0.88 Ma), El Golfo volcano (545−176 ka), and recent rift volcanism (< 158 ka) (Guillou et al. 1996; Carracedo et al. 2001). All these units show evidence of flank landslides: Tiñor (882−545 ka), Las Playas I (545−176 ka) and II (176−145 ka), El Julan (> 160 ka), El Golfo (87−39 ka), and Punta del Norte (unknown age) (Guillou et al. 1996; Day et al. 1997; Carracedo et al. 1999, 2001; Gee et al. 2001; Masson et al. 2002; Acosta et al. 2003; Longpré et al. 2011), which modified their original morphology and had effects on magma plumbing and eruptive dynamics (Manconi et al. 2009) (Fig. 1).

The recent rift volcanism is characterised by the simultaneous activity of three rift arms. During the Holocene, the eruptions are heterogeneously distributed along the NW, S, and NE rifts axes (Rodriguez-Gonzalez et al. 2024) (Fig. 1). At the northwest edge of the coastline, several eruptions are clustered in two areas, Orchilla to the south and El Verodal to the north, whilst minor scattered eruptions are located within the El Golfo embayment (Fig. 1). Vents that mainly erupted tephra are concentrated at the highest part of the El Golfo landslide scar, in the La Cumbre area. Along the S rift axis, fewer vents are slightly scattered in the northern half, El Pinar area, whilst a cluster of more than 20 vents occurs in the southern half, Gorona del Lajial area (Fig. 1). Moreover, in the submarine extension of the S rift, an eruption took place ~2 km offshore during 2011–2012 CE. The NE rift is dominated by a low eruptive activity with scattered eruptions (Fig. 1).

Samples and methods

Sample rationale

A set of 42 Holocene subaerial eruptions were sampled based on the Holocene geological map of El Hierro island (Rodriguez-Gonzalez et al. 2024). The sampling strategy was designed to maximise the representativeness of the erupted volcanic products and to evaluate their spatial variability during the Holocene. We collected lava and tephra samples from the 42 eruptions, including 2 volcanic complexes. These volcanic complexes, named El Lajial and La Restinga (both located at the southern rift), are composed

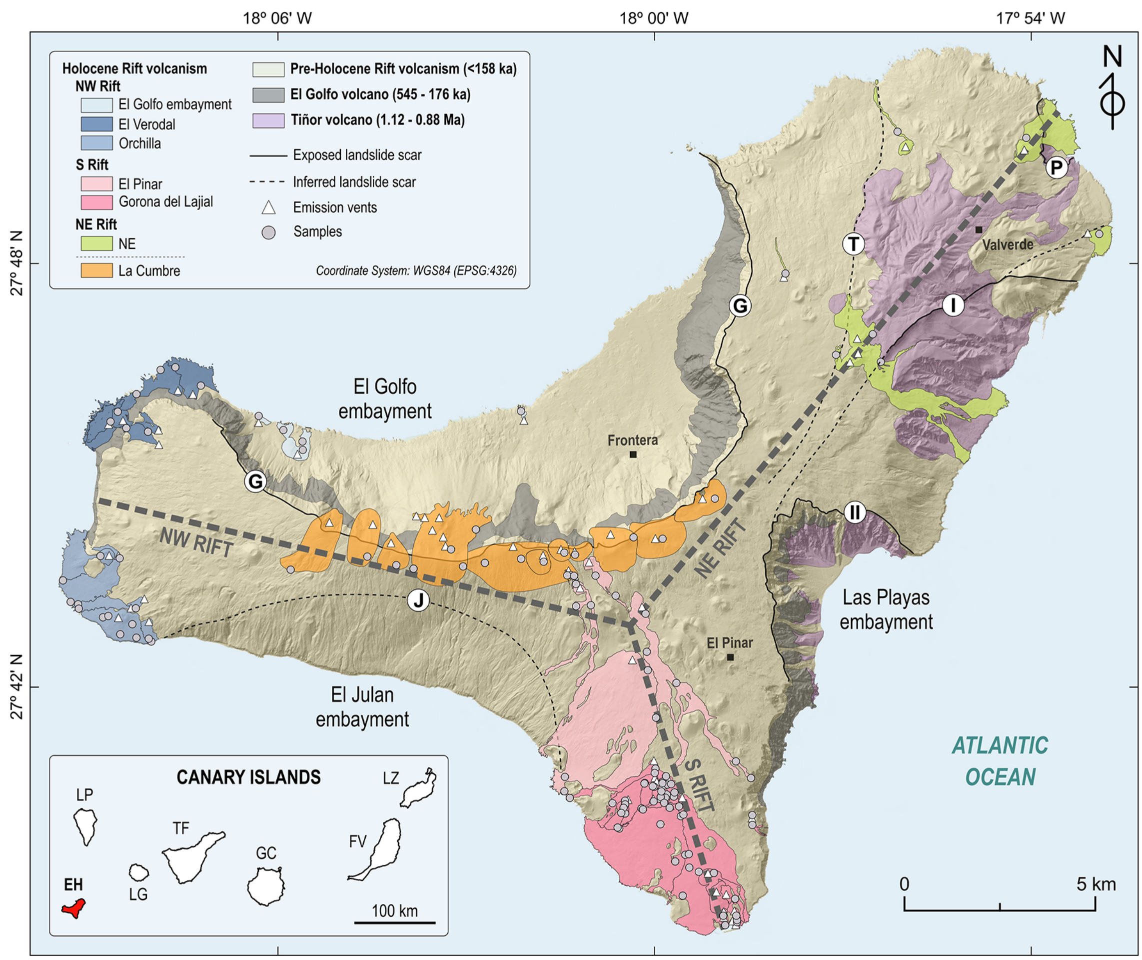

Fig. 1 Geological map of volcanic products cropping out in El Hierro island (adapted from Carracedo et al. 2001; Balcells Herrera et al. 2010a, b; Gómez Sáinz de Aja et al. 2010a, b; Rodriguez-Gonzalez et al. 2024), including the locations of emission vents and the samples investigated in this work (Supplementary Table 1). Holocene eruptions are coloured according to spatial distribution and clustering areas (see text for further explanations). Abbreviations of exposed and inferred landslide scars correspond to Tiñor (T), Las Playas I (I), Las Playas II (II), El Julan (J), El Golfo (G), and Punta del Norte (P). Inset map shows the location of El Hierro (EH) in red within the Canary Islands. Abbreviations for the other islands are Lanzarote (LZ), Fuerteventura (FV), Gran Canaria (GC), Tenerife (TF), La Gomera (LG), and La Palma (LP)

respectively of 15 and 6 construction phases, each of which was sampled individually. After careful hand-specimen revision, 119 samples (98 lavas and 21 tephras) out of 208 were selected for petrographic examination and whole-rock geochemistry. The 64 most representative samples, at least one per eruption, were selected for further textural, mineralogical, and point counting characterisation, as well as for major and minor element quantitative chemical analysis in phenocrysts. In six cases, two samples for a given eruption or construction phase were characterised due to significant differences in their whole-rock geochemistry (Supplementary Tables 1, 2).

Petrographic characterisation

Petrography was carried out using a Zeiss Axiophot optical microscope at the Department of Mineralogy, Petrology and Applied Geology of the University of Barcelona. Point counting was performed to quantify the relative abundance of different components (phenocrysts, groundmass, and vesicles) and the percentage of different minerals constituting the phenocryst population (>0.1 mm in length parallel to the c axis; olivine, clinopyroxene, plagioclase, Fe-Ti oxides, and amphibole). The counting was performed using the JMicroVision v.1.3.4 software (Roduit 2020) on high-resolution thin section scans. For each sample, a lower limit counting of 1000 points in a recursive grid was performed. Results are reported as component assemblage and mineral assemblage in Prieto-Torrell et al. (2024) and Supplementary Table 3. Backscattered electron (BSE) images were acquired using a Scanning Electron Microscope (SEM; Hitachi TM4000 Tabletop Microscope) at the GEO3BCN-CSIC to texturally characterise the groundmass of tephra samples.

Analytical techniques

Whole-rock samples were analysed for major elements by X-ray fluorescence (XRF) using a Philips PW2400 sequential X-ray spectrometer at the Scientific and Technological Centres of the University of Barcelona (CCiTUB). Tephra and lava samples were sawn, then crushed in a jaw crusher, and powdered in a tungsten rings mill. Repeated measurements of reference materials from the Geological Survey of Japan (JB-2 and JB-3) and the United States Geological Survey (BHVO-1) were performed to monitor the precision and accuracy of the analytical determinations. Precision (2σ) was better than ±0.5% and accuracy was better than ±3.4% for all major oxides. Analytical results (Supplementary Table 2) are presented together with literature data from the basanites erupted during the 2011–2012 CE submarine eruption, ~2 km off the southern rift of El Hierro.

Backscattered electron (BSE) images and quantitative chemical analyses in mega-, macro- and mesocryst (*sensu* Zellmer 2021) cores of olivine, clinopyroxene, and plagioclase were determined by Electron Probe Micro-analyser (EPMA) using a JEOL JXA-8230 equipped with five wavelength-dispersive spectrometers (WDS) and one energy-dispersive spectrometer (EDS) at the Scientific and Technological Centres of the University of Barcelona (CCiTUB). Analyses were run using an accelerating voltage of 15 kV, a beam current of 10–15 nA, a peak counting time of 10–30 s, and a focused beam for olivine and clinopyroxene and a beam diameter of 5 µm for plagioclase. Silicate, sulphate, and oxide standards were used to calibrate the instrument prior to each analytical session. For each thin section, five representative areas were defined, in which one macrocryst and one mesocryst of all minerals were analysed, whenever present. More than one type of phenocryst was analysed when significant differences (texture and/or zoning) were observed within the same thin section area. This methodology was employed for EPMA analyses to avoid bias in the number of crystals analysed (Supplementary Tables 4–10).

Thermodynamic modelling

Crystallisation trends were simulated using the thermodynamic modelling software rhyolite-MELTS v.1.2.0 (Gualda et al. 2012). Equilibrium and fractional crystallisation processes were tested using the highest-MgO sample without crystal accumulation signs, as a best approximation of the composition of an original melt (tephra HIR-145, ~10 wt% MgO and 3 vol% phenocrysts, see Supplementary Tables 2, 3). Model conditions were tested for a range of (i) pressures (3, 4, 5, 6, and 7 kbar), (ii) H_2O contents (0, 0.5, 1, 1.5, and 2 wt% H_2O), and (iii) oxygen fugacities, including nickel-nickel oxide (NNO) and absent oxygen fugacity buffer after calculating Fe^{2+}/Fe^{3+} partitioning at NNO. For discussion, we have considered only selected fits (Supplementary Material Figs. S1–S6), whereas all the models performed are provided in Supplementary Table 11.

Results

Petrography

In this section, we provide an overall textural and mineralogical assessment of the Holocene volcanic products investigated at El Hierro island. The term phenocryst is used here in a purely textural sense, without genetic connotations, describing conspicuous crystals much larger than the groundmass and thus easy to distinguish (Iddings 1892;

Zellmer 2021). Within the phenocryst category, mega-, macro- and mesocrysts are further distinguished following the grain size threshold (≥10 mm, 10–0.5 mm, and 0.5–0.1 mm in length parallel to the c axis, respectively) as suggested by Zellmer (2021). Modal abundances of a given phenocryst phase are always reported with respect to other phenocrysts. For full details on the petrography and modal abundances of each of the investigated eruptions, the reader is referred to the dataset reported by Prieto-Torrell et al. (2024).

Textural characterisation

For petrographic evaluation, lava and tephra samples were divided into three groups based on the modal abundance of mega-, macro- and mesocrysts as: (1) aphyric to sub-aphyric (≤5 vol% phenocrysts), (2) porphyritic (5–30 vol% phenocrysts), and (3) ankaramitic (≥30 vol% phenocrysts) (Figs. 2, 3A) (Supplementary Tables 2, 3). Aphyric to sub-aphyric rocks represent ~39% of the Holocene subaerial eruptions and construction phases on El Hierro and mainly crop out as tephra deposits (scoria and pumice) in the La Cumbre area. In addition, minor occurrences of aphyric to sub-aphyric lavas have also been identified in the NW and S rifts (Fig. 2). Porphyritic lavas are, however, the most abundant type of eruption product, representing ~55% of the investigated eruptions and construction phases. They are present in nearly all areas, with the highest number being hosted in the S rift (mainly in the Gorona del Lajial area) (Fig. 2). Ankaramitic lavas are scarce with about 6% of the investigated eruptions and construction phases, and occur in the NW and S rifts (El Verodal and El Pinar areas, respectively) (Fig. 2). Overall, no correlations are present between the altitude above sea level and the crystal content of the investigated samples, as revealed, for instance, by the occurrence of ankaramitic eruptions at low (50 masl) and high (980 masl) altitude (Supplementary Material Fig. S7).

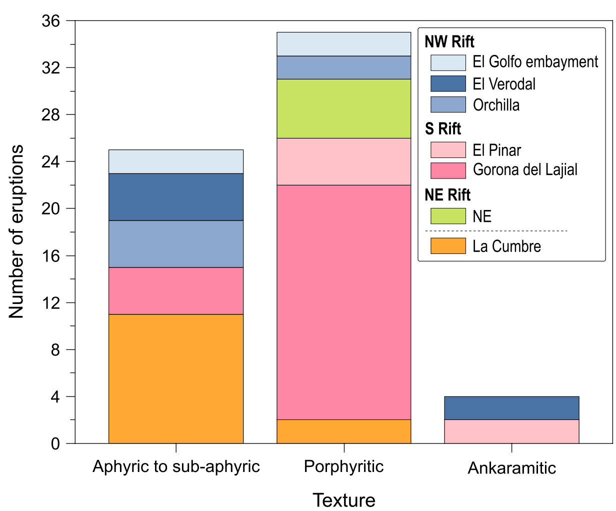

Fig. 2 Stacked column graph showing the number of eruptions in each area according to their texture (based on the modal abundance of phenocrysts). Note that if a single eruption is represented by more than one texture type (i.e., aphyric to sub-aphyric and porphyritic) in the specimens examined, it is counted once for each texture. Construction phases (i.e., forming El Lajial and La Restinga volcanic complexes) are counted here as individual eruptions. Raw data are available in Supplementary Tables 2 and 3

Holocene subaerial lava samples are characterised by the widespread absence of glass in the groundmass, classifying them as holocrystalline. Lavas are massive to highly vesicular (1–57% vesicles) and typically porphyritic (Fig. 2), containing a common phenocryst assemblage of olivine + clinopyroxene + Fe-Ti oxides with variable modal abundances in nearly all investigated samples. Plagioclase as a phenocryst phase occurs alongside variable proportions of olivine, clinopyroxene, and Fe-Ti oxides in eleven samples, typically sub-aphyric. Amphibole phenocrysts are very rare, and occur only in one lava sample from the NW rift and in two pumice samples from the La Cumbre area (Supplementary Table 3). The groundmass of lava samples is mostly pilotaxitic (Fig. 3C–F), and consists of clinopyroxene, Fe-Ti oxides, plagioclase, and minor olivine crystals in varying proportions, although a few samples exhibit either a fine-grained or a trachytic pilotaxitic groundmass (Fig. 3B, G).

Tephra samples show the same phenocryst assemblage as the lavas but with evident glass in the groundmass, which classifies them as hypocrystalline to hypohyaline depending on their degree of crystallinity. Scoria and pumice samples are mainly composed of juvenile fragments, with lithic fragments being subordinate in the studied tephras. We analysed and identified three types of juvenile fragments based on the groundmass texture: (1) sideromelane, (2) tachylite, and (3) intermediate (Fig. 4). The sideromelane fragments are the most abundant, consisting of light yellow to brownish glass under optical microscope (Fig. 4A) and nearly microlite-free pristine glass in BSE images. Tachylite fragments are composed of a dark groundmass under optical microscope (Fig. 4C), with a dense population of sub-microscopic Fe-Ti oxide crystals that embed plagioclase and minor clinopyroxene microlites in BSE images. The intermediate fragments, the least abundant, have a dark-brown groundmass under optical microscope (Fig. 4B) and contain halfway amounts of glass and sub-microscopic Fe-Ti oxide crystals in BSE images respect to sideromelane and tachylite fragments.

Mineralogical characterisation

Olivine occurs as macrocrysts, mesocrysts, and as a minor groundmass phase. Phenocrysts are found both as isolated crystals (Fig. 3C–E) up to 5.8 mm and, in less abundance, as monomineralic to polymineralic clots with clinopyroxene

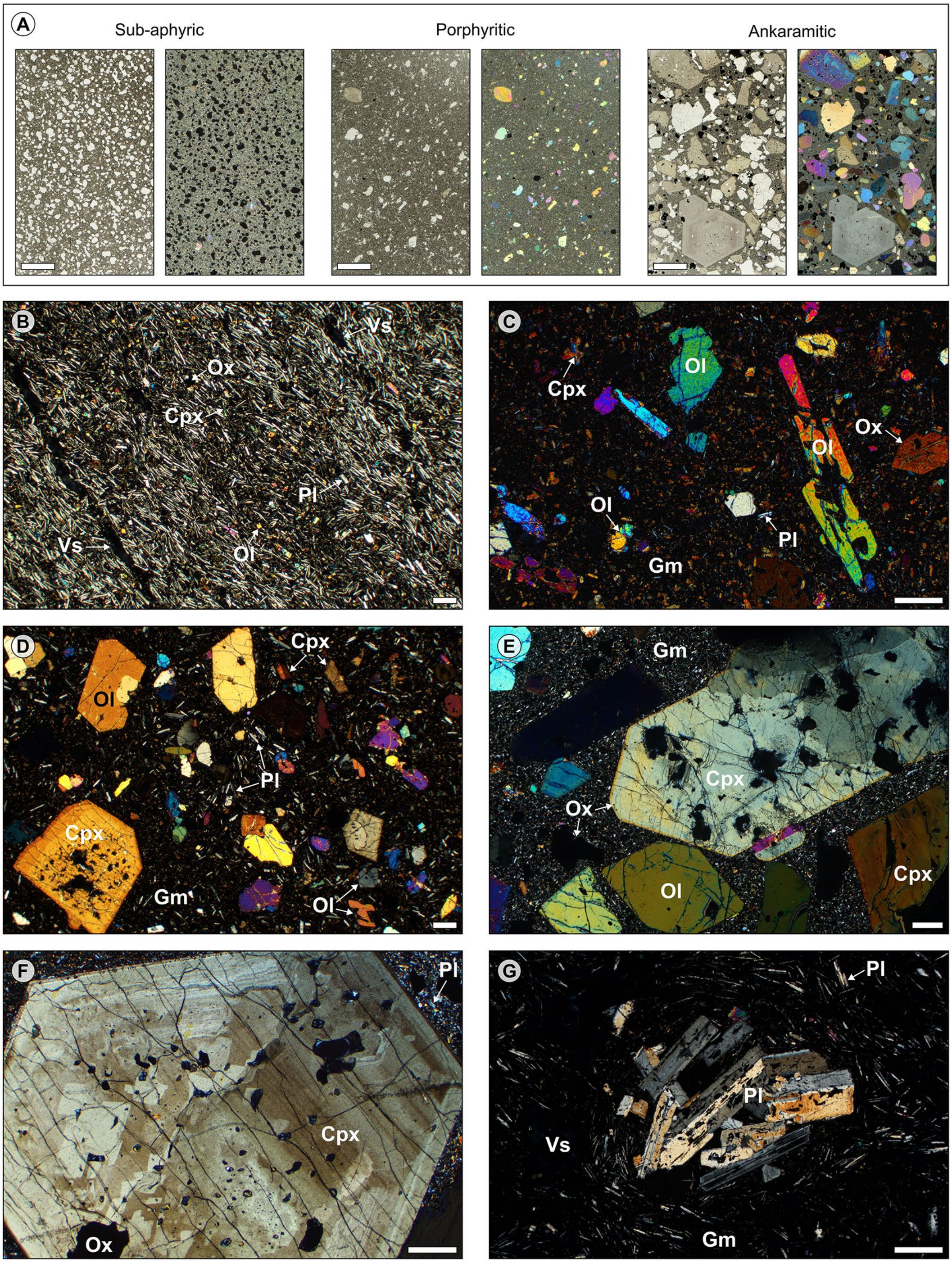

Fig. 3 Summary of petrographic features in Holocene subaerial lavas from El Hierro. Mineral abbreviations following Warr (2021). Scale-bars are 1 cm in panel (A) and 0.5 mm in panels (B–G). (A) High-resolution thin section scans under Plane Polarised Light (PPL; left) and Crossed Polars (XPL; right) of the three texture types occurring at El Hierro (see spatial distributions in Fig. 2). (B–G) All XPL. (B) Aphyric lava showing trachytic texture. (C) Porphyritic lava showing euhedral to anhedral olivine with Fe-Ti oxide inclusions and clinopyroxene glomerocrysts embedded within a clinopyroxene-rich groundmass. (D) Porphyritic lava showing euhedral and subhedral olivine and clinopyroxene crystals, some of the latter with slightly to strongly embayed rims and resorbed cores, embedded within a plagioclase-rich groundmass. (E) Ankaramitic lava showing euhedral to subhedral olivine and clinopyroxene crystals with Fe-Ti oxide inclusions. (F) Detail of a euhedral clinopyroxene megacryst showing resorbed core and complex zoning patterns in an ankaramitic lava. (G) Detail of a monomineralic glomerocryst formed by euhedral to subhedral plagioclase crystals with resorbed cores embedded in a plagioclase-rich groundmass in a sub-aphyric lava. See text for further details

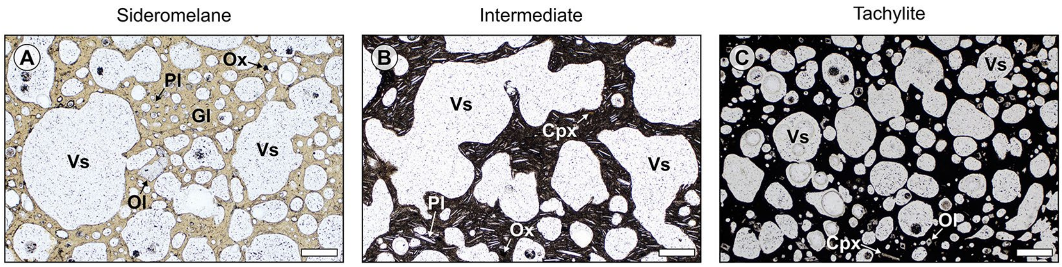

Fig. 4 Petrographic features of sideromelane (A), intermediate (B), and tachylite (C) juvenile fragments identified in the Holocene subaerial tephras from El Hierro, all PPL. Mineral abbreviations following Warr (2021). Scalebar is 0.25 mm in all panels

± Fe-Ti oxides (Fig. 3C). Olivine phenocrysts are either euhedral (Fig. 3E), subhedral to anhedral generally showing slightly to strongly embayed rims (Fig. 3C, D), or skeletal (Fig. 3C). Phenocrysts can display normal to reverse zoning, visible in BSE images, and occasionally host Fe-Ti oxide inclusions in both cores and rims (Fig. 3C). Olivine is mostly subhedral when present as groundmass phase.

Clinopyroxene occurs as megacrysts, macrocrysts, mesocrysts and groundmass phase. Phenocrysts range in size from 0.1 to 5 mm (Fig. 3D), although larger crystals up to 10.3 mm are present in ankaramitic lavas (Fig. 3E, F). Euhedral megacrysts and euhedral to subhedral macrocrysts show resorbed cores (Fig. 3D, F). Macro- and mesocrysts generally occur as isolated euhedral and subhedral crystals, some of the latter with slightly to strongly embayed rims (Fig. 3D), or more rarely as crystal clots (Fig. 3C). Normal to reverse, oscillatory, complex, or sector zoning patterns are present in nearly all crystals, sometimes overprinting each other (Fig. 3D–F). Fe-Ti oxide inclusions are common and, occasionally, smaller ones are concentrated along the outermost zoned rims (Fig. 3E). In the groundmass, clinopyroxenes are euhedral to subhedral and their modal abundances respect to other groundmass components are highly variable (cf. Fig. 3C and D).

Plagioclase mainly occurs as groundmass phase, and as macro- and mesocrysts in some samples. Phenocrysts are up to 4 mm in size, generally euhedral to subhedral, and occur either isolated or as monomineralic glomerocrysts. They sometimes display resorbed cores, Fe-Ti oxide inclusions, as well as oscillatory or complex zoning patterns (Fig. 3G). In the groundmass, plagioclase is mostly present as euhedral laths and occasionally shows preferred orientations defining trachytic textures (Fig. 3B, G).

Fe-Ti oxides occur as mesocrysts, groundmass phase, and minor macrocrysts. Macro- and mesocrysts are euhedral to anhedral isolated crystals with sizes up to 2 mm, some of them exhibiting slightly to strongly embayed rims (Fig. 3E). Mesocrysts are sometimes found as crystal clots, whilst anhedral macrocrysts rarely show skeletal textures. Euhedral to anhedral Fe-Ti oxides, sometimes relatively equidimensional, are present as a groundmass phase.

Amphibole is present as isolated macro- and mesocrysts up to 1.7 mm in size. Phenocrysts are euhedral to subhedral with slightly embayed rims in tephras, whilst anhedral crystals with reaction rims, mainly formed by fine Fe-Ti oxides, are found in lavas.

Whole-rock geochemistry

Whole-rock compositions of the Holocene eruptive products of El Hierro define an alkaline trend from picrites to trachytes (~40–62 wt% SiO_2) in the Total Alkali-Silica diagram of Le Bas et al. (1986). Most of the samples fall within the basanite/tephrite field, being generally basanites (Supplementary Table 2). The trend shows a compositional gap at ~52–60 wt% SiO_2 that isolates the most evolved materials (trachytic pumices), those of the La Cumbre area (Fig. 5A). Lava and tephra samples range from 0.8 to 15.4 wt% MgO, which shows a negative correlation with SiO_2 (Fig. 5B) and Al_2O_3 (Fig. 5C), a positive correlation with FeO^T (Fig. 5E), and a positive correlation with CaO and TiO_2 between 0.8 and 7 wt% MgO followed by a negative correlation up to 15.4 wt% MgO (Fig. 5D, F). The geochemical trends of most major elements show, noteworthy, either smooth (Fig. 5C) or marked (Fig. 5B, D–F) changes in the slope at values of ~7 wt% MgO. At higher concentrations of ~10 wt% MgO, correlation shifts exhibit a decrease of SiO_2 and Al_2O_3 and an increase of CaO, FeO^T, and TiO_2 contents (Fig. 5B–F).

The investigated Holocene subaerial eruptions show variations in whole-rock major element composition depending on their texture and spatial distribution (Fig. 5). Three compositional groups are identified: (i) a main cluster that comprises ankaramitic and most of the porphyritic lavas with ~10–15 wt% MgO, (ii) a second cluster mainly consisting of aphyric to sub-aphyric lava and tephra samples with ~3–10 wt% MgO, and (iii) a more evolved cluster composed of minor trachytic eruptions with ~1 wt% MgO. In this regard, compositional heterogeneities occur in all rifts, even within the same area (e.g., El Verodal in the NW rift). Further details can be found in the Supplementary Material.

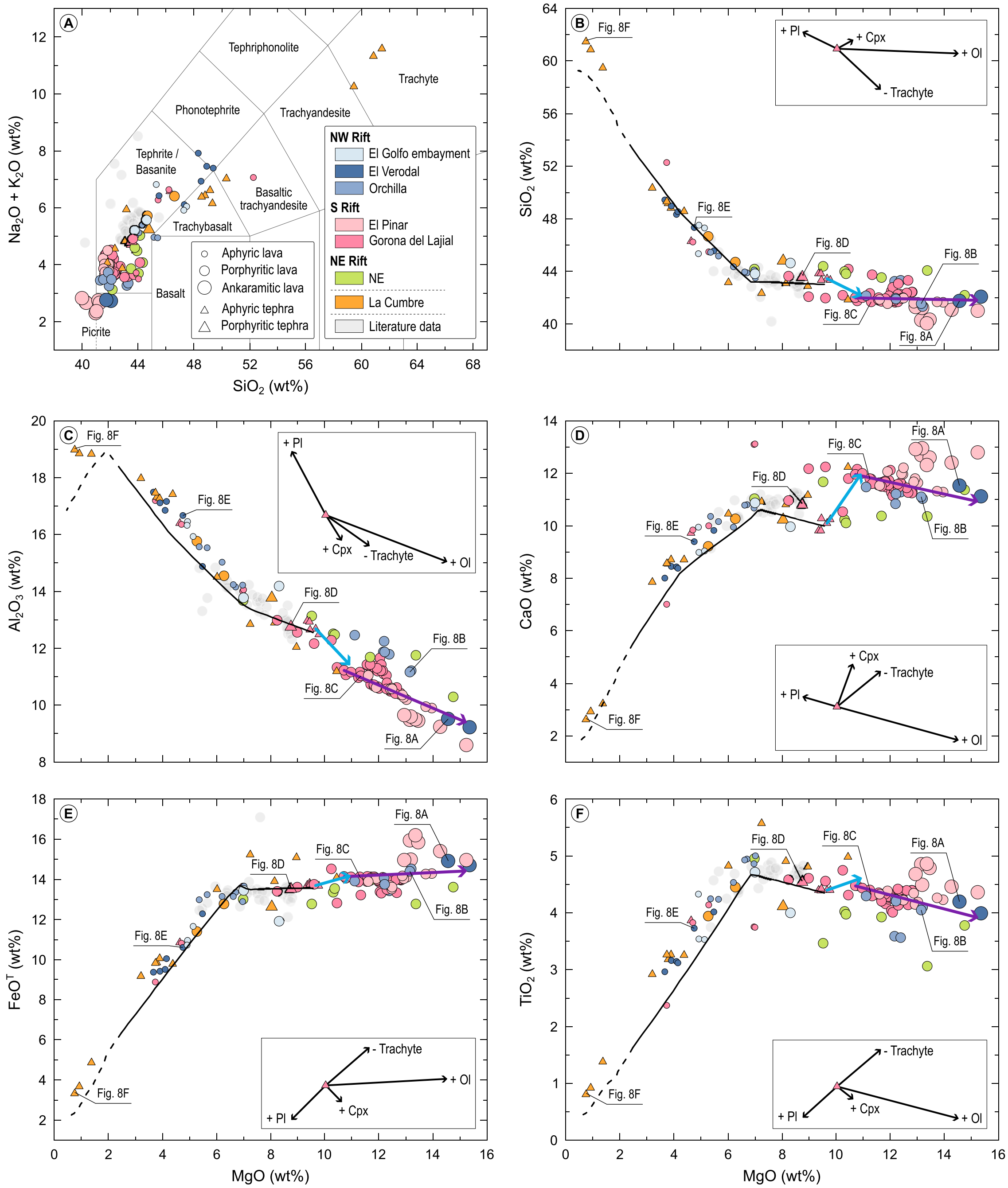

Fig. 5 Whole-rock major element composition of the Holocene subaerial lava and tephra samples investigated in this work (coloured symbols) and submarine lava samples (2011–2012 CE; Tagoro volcano) compiled from the literature (grey symbols) (PEVOLCA 2011; Perez-Torrado et al. 2012; Martí et al. 2013; Longpré et al. 2014; Meletlidis et al. 2015; Rodriguez-Losada et al. 2015). Major elements were normalised to 100 wt% (anhydrous) with Fe distributed between FeO and Fe_2O_3 according to Middlemost (1989). (A) Total Alkali-Silica (TAS) chemical classification (after Le Bas et al. 1986). (B–F) Representative bivariate plots of SiO_2 (B), Al_2O_3 (C), CaO (D), FeO^T (E), and TiO_2 (F) against MgO wt%. Raw data are available in Supplementary Table 2. Solid black line represents fractional crystallisation modelling at 4 kbar, 1 wt% H_2O, and NNO oxygen fugacity buffer from a sub-aphyric tephra with ~10 wt% MgO (sample HIR-145); transition to the dashed black line represents the conditions under which the model becomes unreliable due to the onset of two-pyroxene crystallisation, which is not observed in the investigated eruptive products of El Hierro. Inset boxes within each panel show the effect on whole-rock composition (relative to sample HIR-145) after accumulation (+15 wt% each) of olivine (Ol), clinopyroxene (Cpx), and plagioclase (Pl) crystals and extraction (-15 wt%) of melt with trachytic composition, as calculated through mass balance modelling. This 15 wt% value was chosen based on the maximum olivine accumulation calculated through mass balance. See the discussion section and Supplementary Tables 11 and 12 for more details on mass balance and fractional crystallisation modelling. Error bars are within the size of symbols

Textural and geochemical spatial heterogeneities

Spatial heterogeneities regarding the texture (Fig. 6A) and whole-rock geochemistry (Fig. 6B, C) of the investigated Holocene volcanic products are present throughout El Hierro (see detailed summaries in Supplementary Tables 7–10). The large sample set in the present work has allowed to discriminate such variations with a high temporal and spatial resolution, sometimes even within the same area (Fig. 5). The observed pattern can thus be used to gain insight into the generation of evolving melt compositions, changes in eruptive style, and the dynamics of magmatic plumbing system architecture (discussed in subsection "Melt extraction").

Aphyric to sub-aphyric products (≤5 vol% phenocrysts) are located in the La Cumbre area and the NW rift, and more scarcely in the S rift (Gorona del Lajial area) (Fig. 6A). These eruptions show highly variable SiO_2 and MgO contents ranging between ~42–61 wt% and ~1–10 wt%, respectively (Fig. 6B, C). The highest SiO_2 concentrations

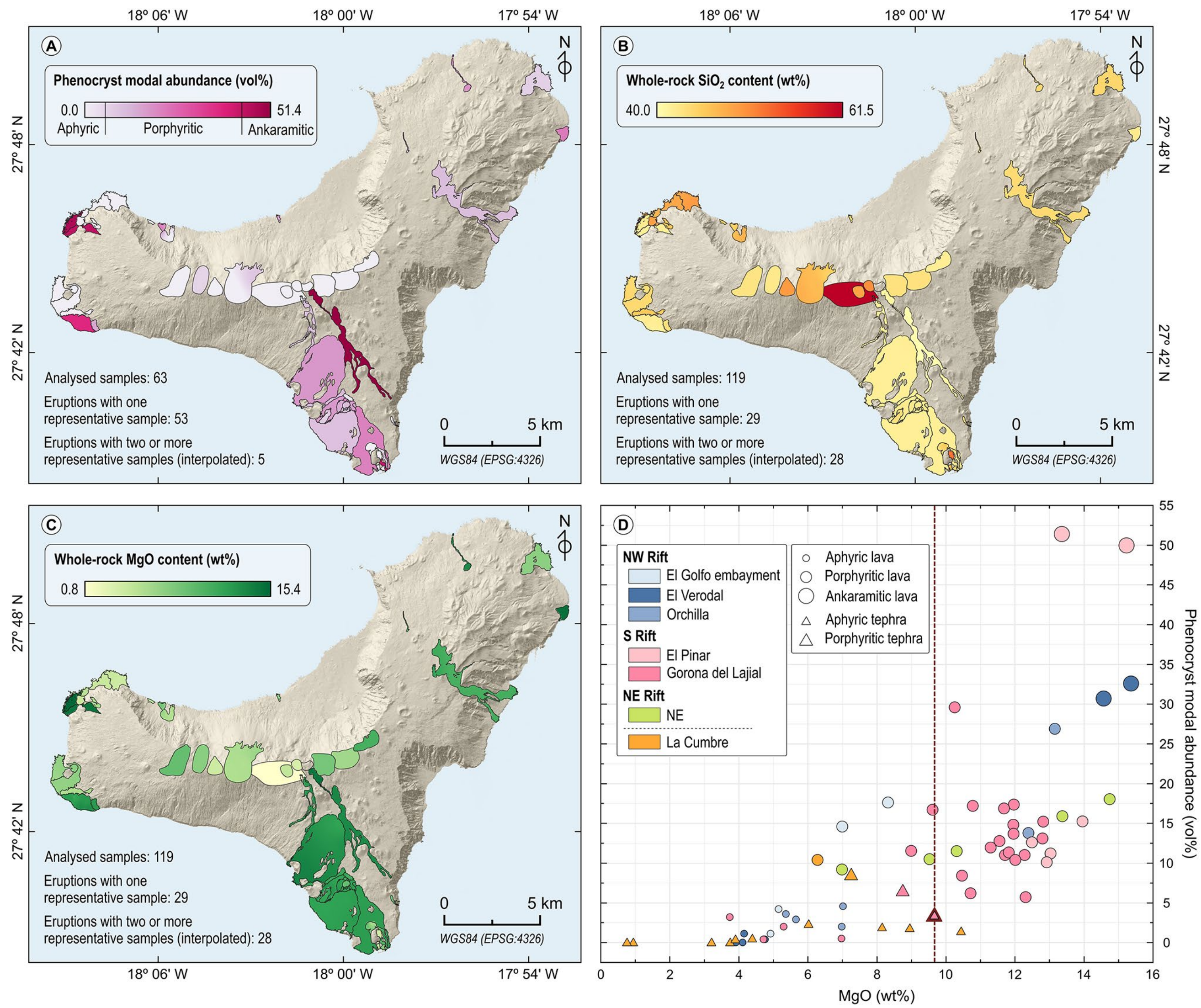

Fig. 6 Spatial distribution of phenocryst modal abundance (i.e., texture) (A), whole-rock SiO_2 (B), and MgO contents (C) of the 42 Holocene eruptions at El Hierro. (D) Bivariate plot of the wt% MgO against the vol% phenocryst content of the 64 most representative lava and tephra samples; the triangle highlighted in maroon represents the initial melt composition used for thermodynamic modelling. Phenocrysts modal abundance data in map (A) and plot (D) were obtained through image analysis on representative thin sections; the complete point counting results of component and mineral assemblages are available in Prieto-Torrell et al. (2024) and in Supplementary Table 3. For eruptions and construction phases with two or more representative samples (up to 7), Inverse Distance Weighted (IDW) interpolation methods were applied individually within each polygon to obtain interpolated raster layers (one per eruption or construction phase). For eruptions and construction phases with one representative sample, the value of that sample was assigned to all pixels in the corresponding raster layer. Data representation was subsequently harmonised under equal colormap thresholds (continuous interval) for map construction. The total number of represented eruptions or construction phases and samples used for representation and interpolation are provided in each panel

correspond to the La Cumbre trachytic eruptions (Fig. 6B), formed by pyroclastic fall and surge deposits (Fig. 4). However, lower SiO_2 eruptions, corresponding to scoria lapilli fall deposits, are also present in this area. In the NW rift, aphyric to sub-aphyric lavas with low- to moderate-SiO_2 contents (Fig. 6B) alternate with porphyritic (in the El Golfo embayment and Orchilla areas) and ankaramitic lavas (in the El Verodal area). In the Gorona del Lajial area, most of the sub-aphyric products are found within the La Restinga Volcanic Complex.

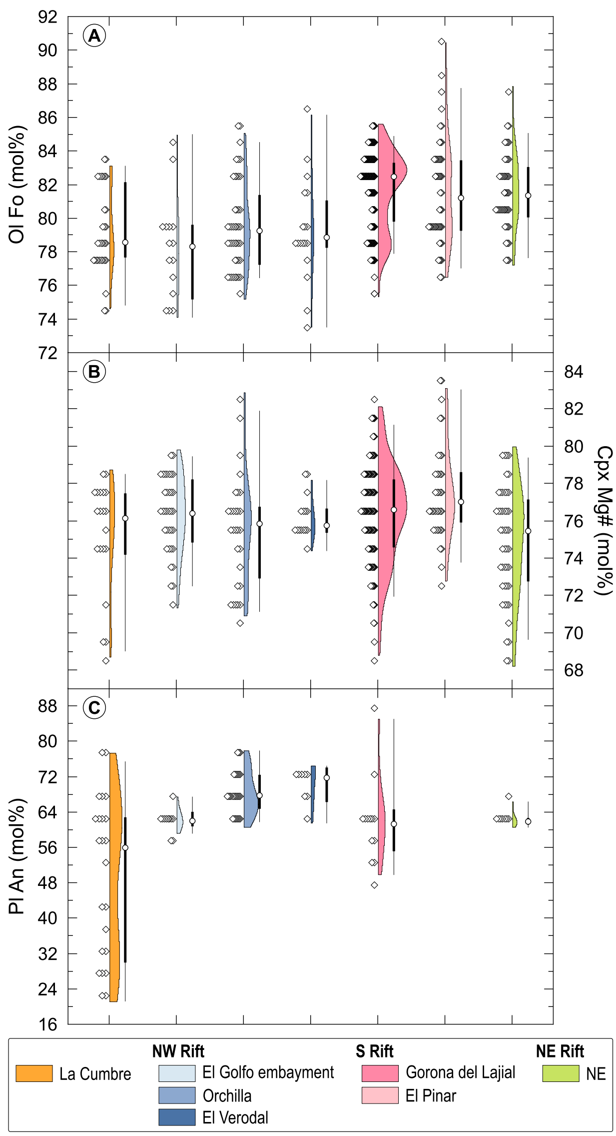

Fig. 7 Distribution of phenocryst core compositions across the seven areas defined in El Hierro (Fig. 1): forsterite (Fo) content of olivine (A), Mg# of clinopyroxene (B), and anorthite (An) content of plagioclase (C). The results are represented as half-violin plots. Data points are on the left (white diamonds) and boxplots are shown on the right. Next to the half-violin illustrations are white circles that show the median values, black boxes are the interquartile ranges (Q1 and Q3), and black whiskers represent 95% confidence interval of the data distribution. Distributions curves are Kernel Density Estimations (KDEs) produced using Scott bandwidth. Raw data are available in Supplementary Tables 4–6

Porphyritic products (5–30 vol% phenocrysts) are mostly located in the NE and S rifts, and more scarcely in the NW rift (El Golfo embayment and Orchilla areas) (Fig. 6A). They show variable whole-rock compositions with SiO_2 contents of ~41–47 wt% (Fig. 6B) and MgO values that range between ~5–15 wt% (Fig. 6C). Isolated porphyritic eruptions occur in the NE rift and within the El Golfo embayment. Porphyritic lavas are the dominant texture in the S rift, where they show homogeneous whole-rock geochemical compositions (Fig. 6B, C).

Ankaramitic lavas (≥30 vol% phenocrysts) are exclusively found in the NW (El Verodal area) and S rifts (El Pinar area) (Fig. 6A) and represent denser and crystal-rich magmas (Figs. 2, 3A, E, F, 5). They have endmember whole-rock geochemical compositions, with the lowest SiO_2 (~40–42 wt%) and highest MgO (~13–15 wt%) contents recorded in the Holocene volcanic products of El Hierro island (Fig. 6B, C). Overall, ankaramitic and most of the porphyritic lavas have phenocryst contents above ~10 vol% and ~10 wt% MgO. In contrast, aphyric to sub-aphyric and a small number of porphyritic lava and tephra samples have MgO contents below ~10 wt% (Fig. 6D).

Mineral chemistry

Mega-, macro- and mesocryst core compositions of olivine, clinopyroxene, and plagioclase across the seven distinguished areas on El Hierro (Fig. 1) are summarised in Fig. 7. The number of phenocryst cores analysed was kept constant for all eruptions and construction phases. The complete EPMA dataset is provided in Supplementary Tables 4–6 (see detailed summaries in Supplementary Tables 7–10). Extended descriptions on mineral chemistry are provided in Supplementary Material.

Olivine phenocryst core compositions of sub-aphyric, porphyritic, and ankaramitic samples range in forsterite (Fo) content [$Fo=100*Mg/(Mg+Fe^{2+})$ mol%] from 74 to 83, 74–90, and 78–86, respectively. Two main populations are identified at ~Fo_{78-80} and ~Fo_{83}. Fo content heterogeneities depending on spatial distribution are present in ankaramitic and porphyritic lavas. Ankaramitic lavas from the NW rift (El Verodal area) cover the whole compositional spectrum (Fo_{78-86}), whilst those from the S rift (El Pinar area) exhibit restricted values (Fo_{79-81}). Primitive olivine crystals (Fo_{88-90}) are exclusively found in porphyritic lavas from the S (El Pinar area) and NE rifts (Fig. 7A).

Clinopyroxene phenocrysts are mostly classified as diopside (Morimoto et al. 1988) and have core compositions ranging in Mg# number [$Mg\#=100*Mg/(Mg+Fe^{2+}+Fe^{3+})$ mol%] from 68 to 83 and 74–79 for porphyritic to sub-aphyric and ankaramitic samples, respectively. Clinopyroxene compositions exhibit unimodal distributions with relatively scattered values and show a main population at ~Mg#$_{76–77}$ in all areas (Fig. 7B).

Plagioclase phenocrysts are classified as oligoclase, andesine, labradorite, and bytownite (Deer et al. 2013). Their core compositions range in anorthite (An) content [An=100*Ca/(Ca+Na+K) mol%] from 21 to 77 for sub-aphyric tephras, 50–85 for sub-aphyric lavas, and 59–69 for porphyritic lavas. Plagioclase cores with ~An$_{\leq 40}$ are exclusively found in the trachytic pumices from the La Cumbre area (Fig. 7C).

Discussion

The textures and chemical compositions of erupted minerals are direct witnesses of the magmatic plumbing system in which they have grown, and their study helps to unravel the processes operating beneath volcanically active regions worldwide (e.g., Davidson and Tepley 1997; Humphreys et al. 2006; Chadwick et al. 2007; Jerram and Martin 2008; Albert et al. 2019, 2022; Pelullo et al. 2022; Caracciolo et al. 2023). The petrological and geochemical framework constrained in space and time provided in this study allows us to discuss the magmatic processes that are currently operating in the active volcanic island of El Hierro.

Fractional crystallisation

From major element correlations (Fig. 5) we infer that fractional crystallisation plays a significant role during magmatic evolution beneath El Hierro, as acknowledged in previous studies (e.g., Carracedo et al. 2001). Textural evidence, such as normal zoning patterns in euhedral olivine, clinopyroxene, and plagioclase phenocrysts, also confirm this observation. Among the multiple equilibrium and fractional crystallisation simulations that we have run using different melt conditions (see subsection "Thermodynamic modelling", Supplementary Material Figs. S1–S6 and Supplementary Table 11), the best fit for all major elements (solid black lines in Fig. 5B–F) is a fractional crystallisation model under pressure of 4 kbar (~14 km, at Moho depth; Ranero et al. 1995), 1 wt% H_2O, NNO oxygen fugacity buffer, and an initial composition with ~10 wt% MgO (sample HIR-145; Supplementary Table 2). Models with the same initial conditions, but assuming 0.5 wt% H_2O at 3 kbar or 1.5 wt% H_2O at 5 kbar, also fit relatively well with the major element compositions (see Supplementary Material Fig. S1). The selected best fit model explains the geochemical compositions between ~3–10 wt% MgO, covering aphyric to sub-aphyric (Fig. 8E), as well as a number of the porphyritic lava and tephra samples (Fig. 8D) with phenocryst modal abundances of generally below ~10 vol% (Fig. 6D). A recent study has considered ~7 wt% MgO as a threshold to distinguish between original melts and rock compositions derived from crystal accumulation, based on the most primitive aphyric sample reported in the island (Ubide et al. 2022). After our meticulous study, which considers not only the MgO wt% content of the rocks but also the texture and mineralogy of 42 Holocene eruptions scattered throughout El Hierro, we have documented the existence of aphyric to sub-aphyric tephras with high (~10 wt%) MgO that cannot be explained by crystal accumulation (Figs. 5B–F, 6D). Furthermore, our crystallisation models (Fig. 5B–F) computed from ~10 wt% MgO, overlap the model presented by these authors. When we then consider the relation between the MgO wt% and the crystal content for each eruption (Fig. 6D), we see that lava and tephra samples with <10 wt% MgO fit our simulation of having differentiated by fractional crystallisation. These eruption products are present in all rift zones of the island, but mainly in the NW rift and the La Cumbre area (Figs. 5B–F, 6A, D).

However, crystallisation models cannot explain the occurrence of porphyritic and ankaramitic lavas with >10 wt% MgO content, which show significant compositional scattering for all major element oxides (Fig. 5B–F) as well as textural features typical of crystal cumulates (Fig. 8A–C). Furthermore, fractional crystallisation modelling is unable to explain the origin of the evolved trachytes from the La Cumbre area (Figs. 5B–F, 6B, C, 8F). Additional models were run to reproduce trachyte formation through fractional crystallisation, for instance using a more evolved starting composition at ~5 wt% MgO (sample HIR-013; Supplementary Table 2) and pressures of 2, 3, and 4 kbar. However, no suitable matches were obtained, as these models do not follow the sample trends or imply the crystallisation of two types of clinopyroxenes or orthopyroxene, absent in the investigated eruptive products of El Hierro (see Supplementary Table 11). Thus, rather than representing endmember felsic compositions from a continuous simple closed system fractional crystallisation trend, where no intermediate compositions between ~1.5 and 3 wt% MgO are found, trachytes are instead isolated at MgO contents of 0.8–1.4 wt% (dashed black lines in Fig. 5B–F). Accordingly, other open system processes occurring within the magmatic plumbing system must be invoked and may be the norm, rather than the exception, during the Holocene magmatic evolution beneath El Hierro.

Melt extraction

Several studies have shown textural and geochemical evidence suggesting magma mixing and crystal recycling

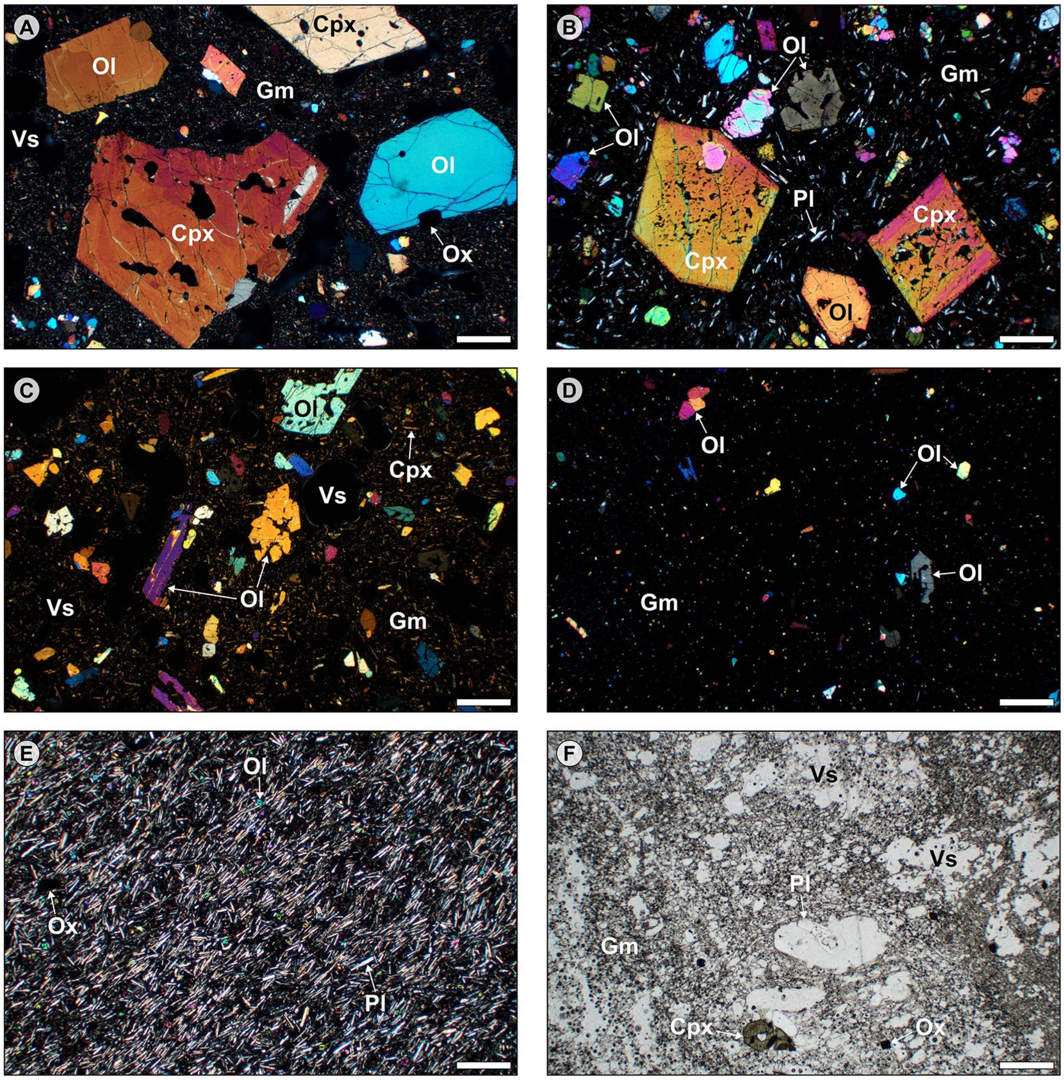

Fig. 8 Textural evidence of the magmatic processes occurring within the crustal mush-dominated plumbing system beneath El Hierro (see major element compositions of representative microphotographs in Fig. 5B–F). Mineral abbreviations following Warr (2021). Scalebar is 1 mm in all panels. Ankaramitic (A) and porphyritic (B, C) lavas with phenocryst modal abundances above ~10 vol% (see Fig. 6D) show disequilibrium (resorbed cores with spongy textures and crystal embayments) and accumulation (monomineralic and polymineralic glomerocrysts) textures, resulting from evolved melt extraction (blue vectors in Fig. 5B–F) and progressive crystal accumulation (purple vectors in Fig. 5B–F). Porphyritic lavas with phenocryst modal abundances below ~10 vol% (D) and aphyric to sub-aphyric products (E) lack disequilibrium and accumulation textures, and follow fractional crystallisation trajectories involving a progressive magmatic evolution (solid black lines in Fig. 5B–F). Periodic extraction of melt with evolved composition from the mush further involves the occurrence of minor trachytic eruptions (F) (Fig. 5B–F) that cannot be explained through simple closed system fractional crystallisation (see main text)

processes at El Hierro (e.g., Stroncik et al. 2009; Martí et al. 2013; Longpré et al. 2014; Taracsák et al. 2019; Ubide et al. 2022) and other OI systems (e.g., Kawabata et al. 2011; Wiesmaier et al. 2011; Zanon et al. 2024). In the samples we investigated, a wide range of zoning types and disequilibrium textures are present in olivine, clinopyroxene, plagioclase, and Fe-Ti oxide crystals, which are commonly interpreted to result from variations in the physicochemical conditions within the plumbing system (e.g., Perugini et al. 2003; Costa et al. 2008). These are, among others, reverse and oscillatory zoning patterns, resorbed cores with rounded shapes or spongy textures, crystal embayments, and reaction rims (Figs. 3C–G, 8A–C, F). Noteworthy are, moreover, the coexistence within the same thin section of (i) strongly resorbed clinopyroxene cores and utterly euhedral clinopyroxene crystals, (ii) skeletal and euhedral olivine crystals with different composition, and (iii) euhedral, normally zoned clinopyroxenes with resorbed cores and reversely zoned clinopyroxenes without resorbed cores (see a complete petrographic characterisation in Prieto-Torrell et al. 2024). Similar textures found in other settings have been shown to be consistent with derivation from transcrustal mush systems after detailed petrological and geochemical investigations (e.g., Geiger et al. 2018; Caracciolo et al. 2020; Mangler et al. 2020; Palummo et al. 2021; Albert et al. 2022).

Two of the main processes governing mush-dominated plumbing systems worldwide are melt extraction and crystal accumulation (e.g., Marsh 2002; Bachmann and Bergantz 2004). When a mush system reaches a critical crystal content (i.e., the melt extraction window) and/or experiences feeding of hotter, permeating recharge magmas, filter pressing or compaction may trigger instabilities yielding to melt extraction (e.g., Marsh 1996; Bachmann and Bergantz 2004, 2006; Dufek and Bachmann 2010; Pistone et al. 2015), fostering crystal accumulation in the leftover mush. At El Hierro, mass balance calculations assuming the extraction of evolved trachytic melt from the composition where our fractional crystallisation model departs (sample HIR-145; Supplementary Table 2), turn out to explain the trend shift at ~10 wt% MgO towards lower SiO_2 and Al_2O_3 and higher MgO, CaO, FeO^T and TiO_2 contents (i.e., the "-Trachyte" vector in the rectangular insets of Fig. 5B–F). After testing this process with different real compositions of the analysed samples (Supplementary Table 12), the trend shift is accurately reproduced by modelling the extraction of 9.3 wt% of trachytic melt (Malpaso sample HIA-2; Fig. 8F; Supplementary Table 2) and the accumulation of 9.4 wt% of clinopyroxene (blue vector in Fig. 5B–F). This model of melt extraction from a mush is consistent with the absence of data points alongside the fractional crystallisation trend between ~1.5 and 3 wt% MgO.

The petrogenesis of the most evolved volcanic products on El Hierro, whose eruption involved explosive felsic volcanism during the Holocene, has remained unexplained hitherto. Our model indicates that these small volumes of felsic (broadly trachytic) eruption products do not result from long-lasting closed system fractional crystallisation in isolated magma reservoirs. More likely, they represent extracted melt fractions from the mush beneath the island. Whether these melt extraction processes occur at the magma underplating zone (≥14 km) or at shallower upper crustal domains has broader implications for volcanic hazard assessment during future eruptions in El Hierro. Comparing these processes with those inferred for the nearby island of La Palma may provide insights into the melt extraction and crystal accumulation depths. In Cumbre Vieja (La Palma), magmas evolve to phonolitic compositions in preferential magma storage zones between the lower curst and the Moho, whereas more primitive magmas differentiate in the upper mantle (Klügel et al. 2015, 2022). The compositional spectrum of historic and prehistoric eruptions at Cumbre Vieja exhibits a semi-continuous trend from basanites/tephrites to phonolites (cf. Fig. 4 in Klügel et al. 2022 and the references therein). This compositional variability agrees with evolved melt extraction at preferential magma storage depths, which likely produced mixing with more mafic magmas resulting in intermediate compositions. In contrast, the Holocene volcanism of El Hierro lacks intermediate compositions with SiO_2 contents between ~52–60 wt%, with trachytes appearing as isolated endmembers (Fig. 5A; see also a similar case reported in Hualālai, Hawaii, Fig. 4A in Shea and Owen 2016). The absence of intermediate compositions suggests that extraction of evolved trachyte melts likely occurs at upper crustal domains, rather than alongside the mafic magmas in the lower crust and upper mantle underplating zone where the trachyte melts would likely mix with more basic magmas. Therefore, in the event of a volcanic crisis where the first precursory signals indicate shallow depths for seismic and geodetic models, without evidence of reactivation of the deep plumbing system, a scenario where melt extraction is occurring and might trigger an explosive felsic eruption should be carefully considered.

Crystal accumulation

The crystal mush leftover after the extraction of evolved melt may further experience strong physicochemical changes (i.e., a crystal mush rejuvenation; e.g., Bachmann et al. 2002; Huber et al. 2012; Petrone et al. 2022). This is remarkably represented in the Holocene volcanism of El Hierro. These changes include shifts in major oxide correlation trends (blue vectors in Fig. 5B–F) and significant textural differences between those samples within the fractional crystallisation trend (Fig. 8D, E) and those that have experienced progressive crystal accumulation after melt extraction (Fig. 8A–C), for instance, by fractional crystallisation from newly supplied magmas into the mush. Modelling olivine and clinopyroxene crystal accumulation starting at the leftover mush composition (sample HIR-082; Supplementary Table 2) fits well with major element correlations at MgO contents between 10.7 and 15.4 wt% (i.e., "+Cpx" and "+Ol" vectors in the rectangular insets of Fig. 5B–F). After testing mass balance calculations with different samples and crystal fractions, the accumulation of 16.1 wt% of olivine, 5.3 wt% of clinopyroxene, and 0.6 wt% of Fe-Ti oxides best fits our sample trends towards the most MgO-rich compositions (purple vector in Fig. 5B–F; Supplementary Table 12). This process is consistent with an increasing number of disequilibrium and accumulation textural evidence (e.g., crystal resorption and monomineralic to polymineralic glomerocrysts) alongside the crystal accumulation trend (Figs. 5, 8A–C), and further explains the progressive, yet noteworthy, increment of the crystal cargo in the cumulates (Fig. 8A–C). Accordingly, we suggest that Holocene lavas with crystal cargoes above ~10 vol% are influenced by crystal accumulation (Fig. 6D). In fact, ankaramitic lavas (Figs. 3A, E, F, 8A) represent accumulation endmembers (Fig. 5B–F) and may be understood as erupted portions from the most crystal-rich regions of the mush. Thus, they are representative of the mush physicochemical properties and should be avoided as the starting composition for crystallisation models (cf. Ubide et al. 2022).

The eruption of ankaramitic lavas, with crystal contents up to 51 vol%, is still a topic to be addressed at El Hierro. According to Manconi et al. (2009), the eruption of ankaramites may be related to the occurrence of giant landslides (i.e., El Golfo landslide; Fig. 1), because such flank collapses may reduce pressure loads above magma reservoirs widening the density window of eruptible magmas. In the NW rift (El Verodal area), an alternating sequence of aphyric and ankaramitic lavas in four stages is accurately exposed (Table 1 and Supplementary Tables 2, 3). This sequential textural evolution within a specific area suggests that spatial heterogeneities in the mush system beneath El Hierro occur not only horizontally (e.g., Fig. 6A–C) but also vertically and temporally. Moreover, this realisation implies that crystallinity variations and significant textural differences in the erupted products might not be related to landslide-induced decompression alone, but reflect a considerable degree of interplay between melt extraction and crystal accumulation processes operating beneath the island (Table 1). Whether the origin of the Holocene ankaramites at El Hierro can be reconciled with the age of the El Golfo collapse (87−39 ka) (Guillou et al. 1996; Carracedo et al. 2001; Longpré et al. 2011), as is the case with the pre-Holocene ankaramites cropping out within the El Golfo embayment (Manconi et al. 2009), would depend on the time span during which the mush system is affected after such a flank collapse, which may last for 10s of kyrs after a lateral collapse (see e.g., Cornu et al. 2021).

Crystals as emissaries of the magmatic plumbing system

The varied crystal core compositions (Fig. 7) and the spatial distribution of textures and whole-rock compositions (Figs. 5, 6) further suggest that the transcrustal mush-dominated plumbing system beneath El Hierro is vertically and horizontally heterogeneous, and that fractional crystallisation, melt extraction, and crystal accumulation are periodic phenomena occurring within it (Fig. 9). Significant textural and chemical differences found in ankaramitic lavas from the S and NW rifts represent good examples of these heterogeneities (Supplementary Tables 3, 4). Ankaramites in the S rift do not show olivine zoning patterns and have restricted Fo core compositions ($Fo_{79–81}$), exhibiting clinopyroxene modal abundances up to three times higher than those of olivine (e.g., Fig. 3E). These facts indicate low perturbation of ankaramitic pods during long residence times before eruption. In contrast, ankaramites in the NW rift generally have the same modal abundances of olivine and clinopyroxene (Fig. 8A) and display reverse zoning and high-Fo olivine cores (up to 86 mol%), suggesting that magma mixing was also involved in their recent magmatic history.

In porphyritic cumulates, vertical heterogeneities are revealed by the high variability in Fo contents of olivine cores (Fig. 7A) (Supplementary Table 4), even within single eruptions, which suggest multiple preferential levels of magma ponding and crystal formation and accumulation that may further undergo magma mixing between them. Moreover, horizontal heterogeneities are revealed by the diversity of the porphyritic products, which show different texture, composition, and magmatic history (Figs. 5, 6) depending on the investigated eruption or construction phase.

In summary, the presence of a complex, heterogeneous transcrustal plumbing system with accumulated mush domains and more liquid portions beneath El Hierro is the most likely scenario to explain the wide range of Holocene eruptive products identified in the island (Fig. 9). The end-member compositions of trachytes (Fig. 8F) (~1 wt% MgO; Fig. 5B–F) and porphyritic cumulates and ankaramites (Fig. 8A–C) (>10 wt% MgO; Fig. 5B–F) lying outside fractional crystallisation trajectories are the result of segregation and subsequent migration of small volumes of highly evolved melt and associated crystal accumulation within the remaining mush system. In contrast, for the mafic magmas, fractional crystallisation is able to produce a spread in compositions between ~3–10 wt% MgO (Figs. 5B–F, 8D, E), which coupled with semi-direct ascent of basic magmas and mixing mechanisms produce the considerable range of zoning types, disequilibrium textures, and the highly variable Fo content observed in olivine cores (Figs. 3, 7A, 8). Our

Table 1 Detail of the alternating aphyric to sub-aphyric and ankaramitic Holocene eruptions in the El Verodal area (NW rift). Eruptions are listed from younger (Lomo Negro) to older (Hoya del Verodal) according to stratigraphic relationships (see Rodriguez-Gonzalez et al. 2024)

Sample name	Type	Texture	Id.	Eruption name	Phenocryst (vol%)	MgO (wt%)
HIR-018	Lava	Ankaramitic	2	Lomo Negro	32.57	15.36
HIR-013	Lava	Aphyric to sub-aphyric	23	Montaña de Marcos	0.40	4.76
HIR-016	Lava	Ankaramitic	24	Montaña de los Guirres	30.70	14.57
HIR-017	Lava	Aphyric to sub-aphyric	25	Hoya del Verodal	0.00	3.92

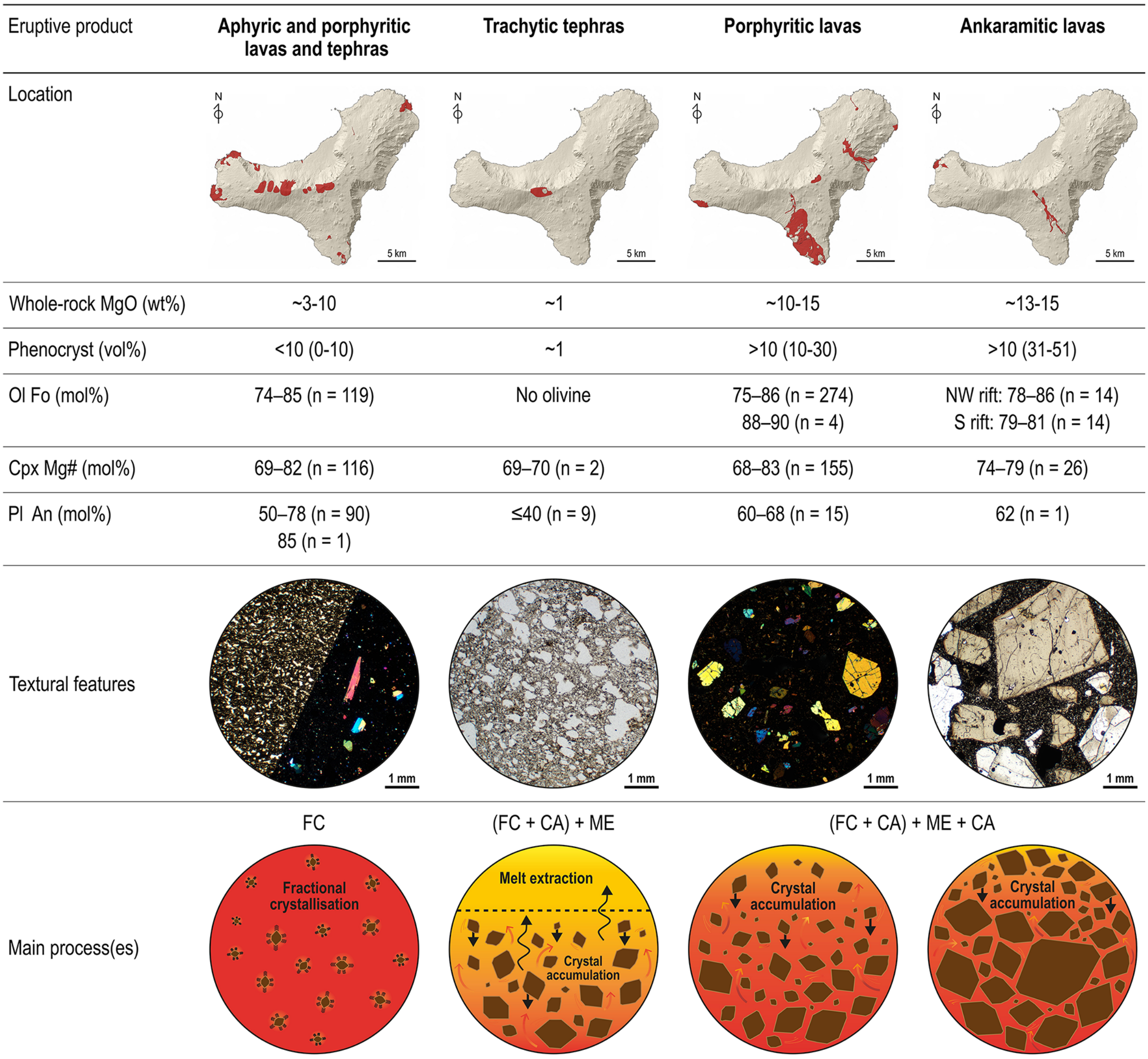

Fig. 9 Summary of the Holocene eruptive products investigated on El Hierro island, including their location, diagnostic whole-rock MgO (wt%) and phenocryst (vol%) contents, phenocryst core compositions (mol%), textural features, and the main magmatic processes involved in their formation. Abbreviations: Ol, olivine; Fo, forsterite; Cpx, clinopyroxene; Pl, plagioclase; An, anorthite; FC, fractional crystallisation; CA, crystal accumulation; ME, melt extraction

interpretation (Fig. 9) is reinforced by the surface distribution and eruptive style variability of the Holocene volcanism throughout the island (Fig. 6A–C). The assessment of these spatial heterogeneities in the mush-dominated system beneath El Hierro, and how they will relate to monitoring data during future unrest episodes, has further implications for volcanic hazard assessment. Ongoing investigations relating these heterogeneities with the pre-eruptive timescales of magma ascent and lateral transport will provide valuable information on the magma pathways feeding eruptions, as previously inferred for other mush-dominated systems at, e.g., Piton de la Fournaise (La Réunion; Albert et al. 2019), Marsili and Stromboli (Tyrrhenian Sea; Petrone et al. 2018; Albert et al. 2022), or the Reykjanes Peninsula (Iceland; Caracciolo et al. 2023).

Conclusions

We provide a new picture of the Holocene volcanism and magmatic plumbing system at El Hierro island. Exhaustive sampling and detailed spatial, petrological, and geochemical characterisation of 42 eruptions offer significant insights into the transcrustal plumbing system. Fractional crystallisation and mass balance modelling unravelled that distinct open-system episodic processes, from evolved melt extraction to the formation of crystal cumulates, are driven by intricate interactions within a complex, vertically and horizontally heterogeneous, transcrustal mush-dominated system. During melt ascent, magma mixing also occurs due to the interception of melt-rich pockets pounded alongside the mush. The new conceptual model of a transcrustal mush dominating the magmatic plumbing system beneath El Hierro explains the spatial variability in magma composition and eruptive style throughout the island. For example, the occurrence of trachytic or dense crystal-rich magmas, and the alternation of aphyric and ankaramitic lavas in the same area. This study not only enhances our understanding of the island's evolution during the Holocene, which is representative of its current and potential future volcanic behaviour, but also provides a valuable framework for investigating similar processes and plumbing system dynamics in other OI settings worldwide. Moreover, it highlights the importance of understanding the vertical and horizontal distribution of mush-dominated systems and how they will impact on future volcanic unrest signs, and thus lead to an improved volcanic monitoring interpretation and hazard assessment.

Supplementary Information The online version contains supplementary material available at https://doi.org/10.1007/s00410-025-02216-6.

Acknowledgements We acknowledge the insightful and constructive comments provided by two anonymous referees, as well as editorial guidance by Gordon Moore.

Funding Open Access funding provided thanks to the CRUE-CSIC agreement with Springer Nature.
Financial support was provided by Grant PGC2018-101027-B-I00, funded by MCIN/AEI/10.13039/501100011033 and by ERDF 'A way of making Europe'. CPT acknowledges the PhD grant 2021 FISDU 00347 funded by Generalitat de Catalunya. HA is a Serra Húnter Lecturer Professor at the UB. EGE acknowledges funding from the "Consolidación Investigadora" Grant CNS2022-135819 to Maria-Gema Llorens funded by MCIN/AEI/10.13039/50110001103. This research was carried out in the Research Consolidated Groups GEOXiS (Generalitat de Catalunya, 2021 SGR 00262), GEOVOL (Canary Islands Government, ULPGC), and Structure and Dynamics of the Earth (Generalitat de Catalunya, 2021 SGR 00413).

Data availability The data are available in the article and in the Supplementary Materials.

Declarations

Conflict of interests The authors have no relevant financial or non-financial interests to disclose.

References

Acosta J, Uchupi E, Muñoz A et al (2003) Geologic evolution of the Canarian Islands of Lanzarote, Fuerteventura, Gran Canaria and La gomera and comparison of landslides at these Islands with those at Tenerife, La Palma and El Hierro. Mar Geophys Res 24:1–40. https://doi.org/10.1007/s11001-004-1513-3

Albert H, Costa F, Di Muro A et al (2019) Magma interactions, crystal mush formation, timescales, and unrest during caldera collapse and Lateral eruption at ocean Island basaltic volcanoes (Piton de La Fournaise, La Réunion). Earth Planet Sci Lett 515:187–199. https://doi.org/10.1016/j.epsl.2019.02.035

Albert H, Trua T, Fonseca J et al (2022) Time scales of open-system processes in a complex and heterogeneous mush-dominated plumbing system. Geology 50:869–873. https://doi.org/10.1130/G49934.1

Anderson AT, Swihart GH, Artioli G, Geiger CA (1984) Segregation vesicles, gas Filter-Pressing, and igneous differentiation. J Geol 92:55–72. https://doi.org/10.1086/628834

Aulinas M, Gimeno D, Fernandez-Turiel JL et al (2010) Small-scale mantle heterogeneity on the source of the Gran Canaria (Canary Islands) Pliocene–Quaternary magmas. Lithos 119:377–392. https://doi.org/10.1016/j.lithos.2010.07.016

Bachmann O, Bergantz GW (2004) On the origin of crystal-poor rhyolites: extracted from batholithic crystal mushes. J Petrol 45:1565–1582. https://doi.org/10.1093/petrology/egh019

Bachmann O, Bergantz GW (2006) Gas percolation in upper-crustal silicic crystal mushes as a mechanism for upward heat advection and rejuvenation of near-solidus magma bodies. J Volcanol Geotherm Res 149:85–102. https://doi.org/10.1016/j.jvolgeores.2005.06.002

Bachmann O, Dungan MA, Lipman PW (2002) The fish Canyon magma body, San Juan volcanic field, Colorado: rejuvenation and eruption of an Upper-Crustal batholith. J Petrol 43:1469–1503. https://doi.org/10.1093/petrology/43.8.1469

Balcells Herrera R, de Gómez Sáinz JA, Pineda Velasco A (2010a) Mapa Geológico de España Escala 1:25.000, Sabinosa (Isla de El Hierro), Hoja 1105-III. IGME. Segunda Serie (MAGNA)

Balcells Herrera R, de Gómez Sáinz JA, Pineda Velasco A (2010b) Mapa Geológico de España Escala 1:25.000, La restinga (Isla de El Hierro), Hoja 1108-II/I. IGME. Segunda Serie (MAGNA)

Bergantz GW, Schleicher JM, Burgisser A (2015) Open-system dynamics and mixing in magma mushes. Nat Geosci 8:793–796. https://doi.org/10.1038/ngeo2534

Bons PD, Arnold J, Elburg MA et al (2004) Melt extraction and accumulation from partially molten rocks. Lithos 78:25–42. https://doi.org/10.1016/j.lithos.2004.04.041

Boulanger M, France L (2023) Cumulate formation and melt extraction from Mush-Dominated magma reservoirs: the melt flush process exemplified at Mid-Ocean ridges. J Petrol 64:1–20. https://doi.org/10.1093/petrology/egad005

Caracciolo A, Bali E, Guðfinnsson GH et al (2020) Temporal evolution of magma and crystal mush storage conditions in the Bárðarbunga-Veiðivötn volcanic system, Iceland. Lithos 352–353:105234. https://doi.org/10.1016/j.lithos.2019.105234

Caracciolo A, Bali E, Halldórsson SA et al (2023) Magma plumbing architectures and timescales of magmatic processes during historical magmatism on the Reykjanes Peninsula, Iceland. Earth Planet Sci Lett 621:118378. https://doi.org/10.1016/j.epsl.2023.118378

Carracedo JC, Day SJ, Guillou H, Perez-Torrado FJ (1999) Giant quaternary landslides in the evolution of La Palma and El Hierro, Canary Islands. J Volcanol Geotherm Res 94:169–190. https://doi.org/10.1016/S0377-0273(99)00102-X

Carracedo JC, Rodriguez-Badiola E, Guillou H et al (2001) Geology and volcanology of La Palma and El Hierro, Western Canaries. Estud Geol 57:175–273. https://doi.org/10.3989/egeol.01575-6134

Cashman KV, Sparks RSJ, Blundy JD (2017) Vertically extensive and unstable magmatic systems: A unified view of igneous processes. Science 355:eaag3055. https://doi.org/10.1126/science.aag3055

Chadwick JP, Troll VR, Ginibre C et al (2007) Carbonate assimilation at Merapi volcano, Java, Indonesia: insights from crystal isotope stratigraphy. J Petrol 48:1793–1812. https://doi.org/10.1093/petrology/egm038

Cooper KM (2017) What does a magma reservoir look like?? The Crystal's-Eye. View Elem 13:23–28. https://doi.org/10.2113/gselements.13.1.23

Cornu M-N, Paris R, Doucelance R et al (2021) Exploring the links between volcano flank collapse and the magmatic evolution of an ocean Island volcano: Fogo, cape Verde. Sci Rep 11:17478. https://doi.org/10.1038/s41598-021-96897-1

Costa F, Dohmen R, Chakraborty S (2008) Time scales of magmatic processes from modeling the zoning patterns of crystals. Rev Mineral Geochem 69:545–594. https://doi.org/10.2138/rmg.2008.69.14

Davidson JP, Tepley FJ (1997) Recharge in volcanic systems: evidence from isotope profiles of phenocrysts. Science 275:826–829. https://doi.org/10.1126/science.275.5301.826

Davies GF (1999) Dynamic Earth: plates, plumes and mantle convection, 1st edn. Cambridge University Press

Day SJ, Carracedo JC, Guillou H (1997) Age and geometry of an aborted rift flank collapse: the San Andres fault system, El Hierro, Canary Islands. Geol Mag 134:523–537. https://doi.org/10.1017/S0016756897007243

Dayton K, Gazel E, Wieser P et al (2023) Deep magma storage during the 2021 La Palma eruption. Sci Adv 9:eade7641. https://doi.org/10.1126/sciadv.ade7641

de Gómez Sáinz JA, Balcells Herrera R, Pineda Velasco A (2010a) Mapa Geológico de España Escala 1:25.000, Valverde (Isla de El Hierro), Hoja 1105-II. IGME. Segunda Serie (MAGNA)

de Gómez Sáinz JA, Balcells Herrera R, Pineda Velasco A (2010b) Mapa Geológico de España Escala 1:25.000, Frontera (Isla de El Hierro), Hoja 1105-IV. IGME. Segunda Serie (MAGNA)

Deegan FM, Troll VR, Barker AK et al (2012) Crustal versus source processes recorded in dykes from the Northeast volcanic rift zone of Tenerife, Canary Islands. Chem Geol 334:324–344. https://doi.org/10.1016/j.chemgeo.2012.10.013

Deer WA, Howie RA, Zussman J (2013) An Introduction to the Rock-Forming Minerals, Third edition. The Minerological Society, London

Dufek J, Bachmann O (2010) Quantum magmatism: magmatic compositional gaps generated by melt-crystal dynamics. Geology 38:687–690. https://doi.org/10.1130/G30831.1

Gee MJR, Watts AB, Masson DG, Mitchell NC (2001) Landslides and the evolution of El Hierro in the Canary Islands. Mar Geol 177:271–293. https://doi.org/10.1016/S0025-3227(01)00153-0

Geiger H, Troll VR, Jolis EM et al (2018) Multi-level magma plumbing at Agung and Batur volcanoes increases risk of hazardous eruptions. Sci Rep 8:10547. https://doi.org/10.1038/s41598-018-28125-2

Gualda GAR, Ghiorso MS, Lemons RV, Carley TL (2012) Rhyolite-MELTS: a modified calibration of MELTS optimized for Silica-rich, Fluid-bearing magmatic systems. J Petrol 53:875–890. https://doi.org/10.1093/petrology/egr080

Guillou H, Carracedo JC, Perez-Torrado FJ, Rodriguez-Badiola E (1996) K-Ar ages and magnetic stratigraphy of a hotspot-induced, fast grown oceanic Island: El Hierro, Canary Islands. J Volcanol Geotherm Res 73:141–155. https://doi.org/10.1016/0377-0273(96)00021-2

Hansteen TH, Klügel A, Schmincke H-U (1998) Multi-stage magma ascent beneath the Canary Islands: evidence from fluid inclusions. Contrib Mineral Petrol 132:48–64. https://doi.org/10.1007/s004100050404

Hoernle K, Schmincke H-U (1993) The role of partial melting in the 15-Ma geochemical evolution of Gran Canada: A blob model for the Canary hotspot. J Petrol 34:599–626. https://doi.org/10.1093/petrology/34.3.599

Huber C, Bachmann O, Dufek J (2012) Crystal-poor versus crystal-rich ignimbrites: A competition between stirring and reactivation. Geology 40:115–118. https://doi.org/10.1130/G32425.1

Humphreys ER, Niu Y (2009) On the composition of ocean Island basalts (OIB): the effects of lithospheric thickness variation and mantle metasomatism. Lithos 112:118–136. https://doi.org/10.1016/j.lithos.2009.04.038

Humphreys MCS, Blundy JD, Sparks RSJ (2006) Magma evolution and Open-System processes at Shiveluch volcano: insights from phenocryst zoning. J Petrol 47:2303–2334. https://doi.org/10.1093/petrology/egl045

Iddings JP (1892) On the crystallization of igneous rocks. Bull. Phil. Soc. Wash

Jerram DA, Martin VM (2008) Understanding crystal populations and their significance through the magma plumbing system. Geol Soc Spec Publ 304:133–148. https://doi.org/10.1144/SP304.7

Kawabata H, Hanyu T, Chang Q et al (2011) The petrology and geochemistry of St. Helena alkali basalts: evaluation of the oceanic Crust-recycling model for HIMU OIB. J Petrol 52:791–838. https://doi.org/10.1093/petrology/egr003

Klügel A, Longpré M-A, García-Cañada L, Stix J (2015) Deep intrusions, lateral magma transport and related uplift at ocean Island volcanoes. Earth Planet Sci Lett 431:140–149. https://doi.org/10.1016/j.epsl.2015.09.031

Klügel A, Albers E, Hansteen TH (2022) Mantle and crustal xenoliths in a tephriphonolite from La Palma (Canary Islands): implications for phonolite formation at oceanic Island volcanoes. Front Earth Sci 10:761902. https://doi.org/10.3389/feart.2022.761902

Le Bas MJ, Le Maitre RW, Streckeisen A et al (1986) A chemical classification of volcanic rocks based on the total Alkali-Silica diagram. J Petrol 27:745–750. https://doi.org/10.1093/petrology/27.3.745

Lees JM (2007) Seismic tomography of magmatic systems. J Volcanol Geotherm Res 167:37–56. https://doi.org/10.1016/j.jvolgeores.2007.06.008

Longpré M-A, Chadwick JP, Wijbrans J, Iping R (2011) Age of the El Golfo debris avalanche, El Hierro (Canary Islands): new constraints from laser and furnace 40Ar/39Ar dating. J Volcanol Geotherm Res 203:76–80. https://doi.org/10.1016/j.jvolgeores.2011.04.002

Longpré M-A, Klügel A, Diehl A, Stix J (2014) Mixing in mantle magma reservoirs prior to and during the 2011–2012 eruption at El Hierro, Canary Islands. Geology 42:315–318. https://doi.org/10.1130/G35165.1

Manconi A, Longpré M-A, Walter TR et al (2009) The effects of flank collapses on volcano plumbing systems. Geology 37:1099–1102. https://doi.org/10.1130/G30104A.1

Mangler MF, Petrone CM, Hill S et al (2020) A pyroxenic view on magma hybridization and crystallization at Popocatépetl volcano,

Mexico. Front Earth Sci 8:362. https://doi.org/10.3389/feart.2020.00362
Marsh BD (1996) Solidification fronts and magmatic evolution. Mineral Mag 60:5–40. https://doi.org/10.1180/minmag.1996.060.398.03
Marsh BD (2002) On bimodal differentiation by solidification front instability in basaltic magmas, part 1: basic mechanics. Geochim Cosmochim Acta 66:2211–2229. https://doi.org/10.1016/S0016-7037(02)00905-5
Martí J, Castro A, Rodriguez C et al (2013) Correlation of magma evolution and geophysical monitoring during the 2011–2012 El Hierro (Canary Islands) submarine eruption. J Petrol 54:1349–1373. https://doi.org/10.1093/petrology/egt014
Masson DG, Watts AB, Gee MJR et al (2002) Slope failures on the flanks of the Western Canary Islands. Earth-Sci Rev 57:1–35. https://doi.org/10.1016/S0012-8252(01)00069-1
McKenzie D (1984) The generation and compaction of partially molten rock. J Petrol 25:713–765. https://doi.org/10.1093/petrology/25.3.713
McKenzie D, O'Nions RK (1983) Mantle reservoirs and ocean Island basalts. Nature 301:229–231. https://doi.org/10.1038/301229a0
Meletlidis S, Di Roberto A, Cerdeña ID et al (2015) New insight into the 2011–2012 unrest and eruption of El Hierro Island (Canary Islands) based on integrated geophysical, geodetical and petrological data. Ann Geophys 58:4. https://doi.org/10.4401/ag-6754
Middlemost EAK (1989) Iron oxidation ratios, norms and the classification of volcanic rocks. Chem Geol 77:19–26. https://doi.org/10.1016/0009-2541(89)90011-9
Morimoto N, Fabries J, Ferguson AK et al (1988) Nomenclature of pyroxenes. Am Min 77:1123–1133
Niu Y, Wilson M, Humphreys ER, O'Hara MJ (2011) The origin of Intra-plate ocean Island basalts (OIB): the lid effect and its geodynamic implications. J Petrol 52:1443–1468. https://doi.org/10.1093/petrology/egr030
O'Hara MJ (1998) Volcanic plumbing and the space Problem—Thermal and geochemical consequences of Large-Scale assimilation in ocean Island development. J Petrol 39:1077–1089. https://doi.org/10.1093/petroj/39.5.1077
Palummo F, Mollo S, Petrone CM et al (2021) Decoding multiple zoning patterns in clinopyroxene phenocrysts at Vulcano Island: A record of dynamic crystallization through interconnected reservoirs. Lithos 406–407:106517. https://doi.org/10.1016/j.lithos.2021.106517
Peltier A, Bachèlery P, Staudacher T (2009) Magma transport and storage at piton de La fournaise (La Réunion) between 1972 and 2007: A review of geophysical and geochemical data. J Volcanol Geotherm Res 184:93–108. https://doi.org/10.1016/j.jvolgeores.2008.12.008
Pelullo C, Chakraborty S, Cambeses A et al (2022) Insights into the Temporal evolution of magma plumbing systems from compositional zoning in clinopyroxene crystals from the Agnano-Monte spina plinian eruption (Campi Flegrei, Italy). Geochim Cosmochim Acta 328:185–206. https://doi.org/10.1016/j.gca.2022.04.007
Perez-Torrado FJ, Carracedo JC, Rodriguez-Gonzalez A et al (2012) La Erupción submarina de La restinga En La Isla de El Hierro, Canarias: octubre 2011-Marzo 2012. Estud Geol 68:5–27. https://doi.org/10.3989/egeol.40918.179
Perugini D, Busà T, Poli G, Nazzareni S (2003) The role of chaotic dynamics and flow fields in the development of disequilibrium textures in volcanic rocks. J Petrol 44:733–756. https://doi.org/10.1093/petrology/44.4.733
Petrone CM, Braschi E, Francalanci L et al (2018) Rapid mixing and short storage timescale in the magma dynamics of a steady-state volcano. Earth Planet Sci Lett 492:206–221. https://doi.org/10.1016/j.epsl.2018.03.055
Petrone CM, Mollo S, Gertisser R et al (2022) Magma recharge and mush rejuvenation drive paroxysmal activity at stromboli volcano. Nat Commun 13:7717. https://doi.org/10.1038/s41467-022-35405-z
PEVOLCA (2011) Informe petrológico de la erupción de la isla de El Hierro
Pistone M, Arzilli F, Dobson KJ et al (2015) Gas-driven filter pressing in magmas: insights into in-situ melt segregation from crystal mushes. Geology 43:699–702. https://doi.org/10.1130/G36766.1
Prieto-Torrell C, Aulinas M, Cabrera MC et al (2024) Petrographic dataset of the holocene volcanism on the Island of El Hierro (Canary Islands, Spain). https://doi.org/10.20420/1763.2024.663
Ranero CR, Torne M, Banda E (1995) Gravity and multichannel seismic reflection constraints on the lithospheric structure of the Canary swell. Mar Geophys Res 17:519–534. https://doi.org/10.1007/BF01204342
Rodriguez-Gonzalez A, Fernandez-Turiel JL, Cabrera MC et al (2024) Image dataset of the holocene volcanism on the Island of El Hierro (Canary Island, Spain): stratigraphic relationships. https://doi.org/10.20420/1770.2024.695
Rodriguez-Losada JA, Eff-Darwich A, Hernandez LE et al (2015) Petrological and geochemical highlights in the floating fragments of the October 2011 submarine eruption offshore El Hierro (Canary Islands): relevance of submarine hydrothermal processes. J Afr Earth Sci 102:41–49. https://doi.org/10.1016/j.jafrearsci.2014.11.005
Roduit N (2020) JMicroVision: image analysis toolbox for measuring and quantifying components of high-definition images. Version 1.3.4.
Shea T, Owen J (2016) Discovery of a trachyte ignimbrite sequence at Hualālai, Hawaii. Bull Volcanol 78:34. https://doi.org/10.1007/s00445-016-1027-2
Sisson TW, Bacon CR (1999) Gas-driven filter pressing in magmas. Geology 27:613. https://doi.org/10.1130/0091-7613(1999)027%3C0613:GDFPIM%3E2.3.CO;2
Sparks RSJ, Annen C, Blundy JD et al (2019) Formation and dynamics of magma reservoirs. Philos Trans R Soc A 377:20180019. https://doi.org/10.1098/rsta.2018.0019
Stroncik NA, Klügel A, Hansteen TH (2009) The magmatic plumbing system beneath El Hierro (Canary Islands): constraints from phenocrysts and naturally quenched basaltic glasses in submarine rocks. Contrib Mineral Petrol 157:593–607. https://doi.org/10.1007/s00410-008-0354-5
Taracsák Z, Hartley ME, Burgess R et al (2019) High fluxes of deep volatiles from ocean Island volcanoes: insights from El Hierro, Canary Islands. Geochim Cosmochim Acta 258:19–36. https://doi.org/10.1016/j.gca.2019.05.020
Ubide T, Larrea P, Becerril L, Galé C (2022) Volcanic plumbing filters on ocean-island basalt geochemistry. Geology 50:26–31. https://doi.org/10.1130/G49224.1
Warr LN (2021) IMA–CNMNC approved mineral symbols. Mineral Mag 85:291–320. https://doi.org/10.1180/mgm.2021.43
White WM (2010) Oceanic Island basalts and mantle plumes: the geochemical perspective. Annu Rev Earth Planet Sci 38:133–160. https://doi.org/10.1146/annurev-earth-040809-152450
Wiesmaier S, Deegan FM, Troll VR et al (2011) Magma mixing in the 1100 AD Montaña reventada composite lava flow, Tenerife, Canary Islands: interaction between rift zone and central volcano plumbing systems. Contrib Mineral Petrol 162:651–669. https://doi.org/10.1007/s00410-010-0596-x
Zanon V, Métrich N, D'Oriano C (2024) Geochemical processes in the roots of the Azores magmatic systems. Contrib Mineral Petrol 179:64. https://doi.org/10.1007/s00410-024-02142-z

Zellmer GF (2021) Gaining acuity on crystal terminology in volcanic rocks. Bull Volcanol 83:78. https://doi.org/10.1007/s00445-021-01505-9